

Article

Major, Trace, and Rare-Earth Element Geochemistry of Nb-V Rich Andradite-Schorlomite-Morimotoite Garnet from Ambadungar-Saidivasan Alkaline Carbonatite Complex, India: Implication for the Role of Hydrothermal Fluid-Induced Metasomatism

Amiya K. Samal ¹, Rajesh K. Srivastava ^{1,*} and Dewashish Upadhyay ²

¹ Centre of Advanced Study in Geology, Banaras Hindu University, Varanasi 221005, India; amiyasamal007@gmail.com

² Department of Geology and Geophysics, Indian Institute of Technology (IIT), Kharagpur 721 302, India; dewashish@gg.iitkgp.ac.in

* Correspondence: rajeshgeolbhu@gmail.com or rajeshgeolbhu@bhu.ac.in

Abstract: In situ major, trace and rare-earth element composition of Ti-rich garnets from Ambadungar-Saidivasan alkaline carbonatite complex (ASACC) are presented to constrain its likely genesis. The garnets are characterized by high andradite (42.7–57.3), schorlomite (22.0–31.0), and morimotoite (15.6–26.5) end members. No distinct chemical zonation is noticed except for minor variations in Ti content. The garnets are enriched in LREE (average 731 ppm) and relatively depleted in HREE (average 186 ppm) and show an M-type first tetrad that leads to a convex upward pattern between Ce and Gd. Mildly positive to no Eu anomalies are observed ($\text{Eu}/\text{Eu}^* = 1.06\text{--}1.17$). The REE patterns ($\text{La}_N/\text{Yb}_N = 1.11\text{--}2.11$) are similar to those of garnets from skarn deposits. The presence of tetrad effect in the LREE pattern suggests an active role of metasomatic processes involving hydrothermal fluids during the growth of the garnets. These garnets also contain high Nb (282–2283 ppm) and V (1083–2155 ppm) concentrations, which stand out against the composition of the host rock. Therefore, late-stage metasomatic reactions of earlier formed minerals with hydrothermal fluid enriched in Fe, Si, LREE, Nb, V, and Ti led to the formation of garnet. The primary source for these elements could be magnetite, ilmenite, and pyrochlore present in different varieties of carbonatites in the ASACC, with the required elements being released during their interaction with the hydrothermal fluid. The hydrothermal fluid was likely to be moderately acidic, and having fluoride and sulfate as the primary ligands.

Keywords: Ti-rich garnet; andradite-schorlomite-morimotoite; REE; Ambadungar-Saidivasan; carbonatite agglomerate/breccia; metasomatism



Citation: Samal, A.K.; Srivastava, R.K.; Upadhyay, D. Major, Trace, and Rare-Earth Element Geochemistry of Nb-V Rich Andradite-Schorlomite-Morimotoite Garnet from Ambadungar-Saidivasan Alkaline Carbonatite Complex, India: Implication for the Role of Hydrothermal Fluid-Induced Metasomatism. *Minerals* **2021**, *11*, 756. <https://doi.org/10.3390/min11070756>

Academic Editor: Vincenza Guarino

Received: 28 May 2021

Accepted: 11 July 2021

Published: 13 July 2021

Publisher's Note: MDPI stays neutral with regard to jurisdictional claims in published maps and institutional affiliations.



Copyright: © 2021 by the authors. Licensee MDPI, Basel, Switzerland. This article is an open access article distributed under the terms and conditions of the Creative Commons Attribution (CC BY) license (<https://creativecommons.org/licenses/by/4.0/>).

1. Introduction

The garnet supergroup comprises orthosilicate minerals that include twenty-one end-members found in a variety of geological environments [1,2]. Garnet is a characteristic mineral found in many metamorphic rocks as well as in some granites, pegmatites, and alkaline and felsic volcanic rocks [3]. The mineral usually preferentially incorporates the heavy rare earth elements (HREE) during growth resulting in high Lu/Hf and Sm/Nd ratios. Garnet-controlled fractionation of the REE is a commonly used geochemical tracer [4]. The incorporation of REE in garnet is controlled by the composition of garnet as well as by the composition of the rock matrix/melt/fluid from which the garnet grows/crystallizes. In many geologic environments involving the presence of fluid phase, external factors such as fluid composition, water/rock (W/R) ratios, dynamics of metasomatism including physicochemical conditions can control the major and trace element chemistry of garnet [4]. The complex process of the partitioning of REE between metasomatic fluid and

growing garnet is primarily guided by crystal chemistry, crystal-fluid equilibrium, growth rate, and surface adsorption (e.g., [4–8]). Therefore, the REE geochemistry of garnet is a potential tool to comprehend the evolution of metasomatic fluids [4]. Although discrimination between igneous and metasomatic andradite-grossularite garnets based on chemical zonation, color and trace element content is challenging, however, for petrological interpretations, it is always indispensable to classify whether the garnets are of igneous origin crystallizing from a melt phase or of subsolidus origin growing from a fluid phase during hydrothermal processes [9].

The Ambadungar-Saidivasan alkaline carbonatite complex (ASACC) is one of the several alkaline complexes present within the Chhota Udepur subprovince of the Deccan flood basalt province, Western India, which occur approximately 5–8 km north of the Narmada rift (see Figure 1) (e.g., [10–16]). Besides carbonatite and carbonatite breccia, these complexes also host several alkaline rocks like nephelinite, phonolite, tinguaite, syenite, nepheline syenite [12,17]. Garnets have been reported from most of the felsic rock types of these complexes [17–20]; however, their origin and genesis have not been investigated in detail except for a handful of studies (e.g., [19,20]). Most of the previous studies are primarily based on the major element chemistry of garnet. Based on a limited set of electron microprobe data, compositional variation in zoned melanite phenocrysts from nephelinites of Ambadungar complex has been presented [19]. Similarly, the mineral chemistry of zoned Ti-rich melanite-schorlomite from a tephrite plug in the complex is also discussed [20]. However, due to the lack of trace and rare-earth element data, the genesis of these garnets—whether they are primary magmatic or secondary metasomatic—is still contentious. The prime objective of this work is to provide first-hand rare-earth, trace and major element data on garnets from ASACC to constrain their genesis.

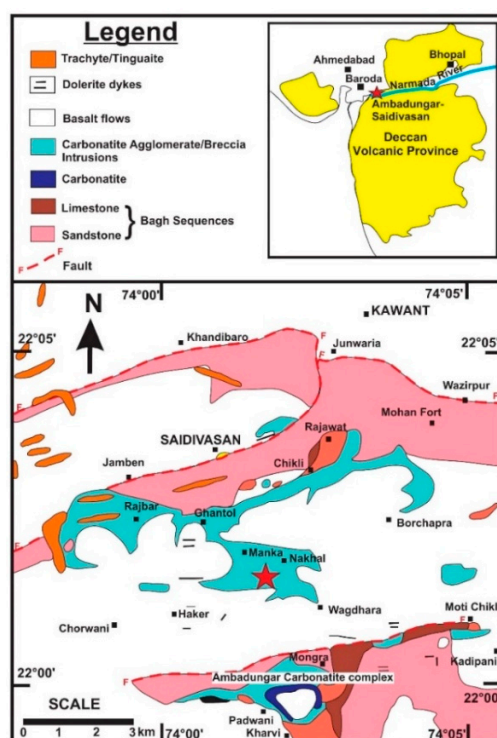


Figure 1. Geological map of the Ambadungar-Saidiwasan alkaline carbonatite complex, modified after [10,12,14,15]. Area of sample locations are marked by a red star. Inset: map shows location of the ASACC.

2. Geological Framework

The Ambadungar alkaline carbonatite complex in western India near the Chhota Udepur region is intrusive into basalts of the Deccan Volcanic Province and cretaceous

rocks of the Bagh formation [18]. A number of other alkaline-carbonatite complexes have been reported from different parts of the entire Indian Shield, and most of them are spatially related with well-defined major tectonic domains (e.g., [13,16,21]). The Ambadungar-Saidivasan alkaline carbonatite complex (ASACC) is tectonically related to the ENE-trending Narmada-Son rift [13,22], and its geological set-up is well studied by several workers (e.g., [11,12,14,16,17,23,24] and references therein).

In general, the ASACC comprises a wide range of carbonatites, genetically associated alkaline rocks, and large sill type exposures of carbonatite agglomeratic/breccia intrusions (see Figure 1) [11,12,14,17]. The carbonatites are texturally and mineralogically classified as sövite, alvikite, ankerite, and brecciated types, whereas chemically, they vary from calcio-, ferro- to silico-carbonatites [11,12,14,25]. Most exposures of carbonatites occur as flows, plugs, and dykes and/or ring dykes, whereas alkaline rocks are exposed as dykes and plugs. The main carbonatite body, which occurs as a large ring structure, is exposed at the Ambadungar village, whereas small exposures are seen all around the region. Petrographic and geochemical characteristics of alkaline rocks classify them as phonolite, tinguaitite, nephelinite, trachyte, and syenite/nepheline syenite, and these are exposed in and around Khadla, Kharvi, Padwani, Mogra, and Kadipani (see Figure 1) [12,17]. The northern part of the complex is extensively covered by carbonatite agglomeratic/brecciated sill intrusions, particularly in and around the Manka-Nakhal-Saidivasan region, consisting of rock fragments of a variety of lithotypes, including basaltic, carbonatitic, tuffisite, sedimentary, and alkaline rocks (see Figure 2). Such exposures are also found in the south of the Ambadungar village as well. A few E–W trending dolerite dykes are also encountered within the Deccan Volcanic Province.



Figure 2. Close views of field exposures of carbonatite agglomeratic/brecciated intrusions. (a) Medium to coarse phenocrysts/xenocrysts/xenoliths embedded within the carbonate matrix exposed near the village Rajawat. (b) Contains larger xenoliths of sedimentary rocks, basalts, carbonatites, alkaline rocks together with xenocrysts/phenocrysts exposed near the village Manka.

The ASACC has been dated by ^{40}Ar – ^{39}Ar method, which suggests its emplacement at ca. 65–68 Ma (e.g., [23,26,27]). A few minerals such as apatite, feldspar, and calcite, extracted from two carbonatite samples and one nephelinite sample from the ASACC, have been dated by U–Pb isotopes and yielded an age of 65.4 ± 2.5 Ma age [28], making them broadly coeval with Deccan volcanism. Other lines of evidence such as field relationships also suggest that the ASACC is intrusive within the Deccan large igneous province (LIP). The alkaline rocks from different alkaline complexes linked with the Narmada-Son rift zone

are contemporaneous with the ASACC and have ^{40}Ar – ^{39}Ar emplacement ages between 65 and 68 Ma [23,29]. Therefore, this suggests their emplacement either synchronous with the main Deccan LIP event or pre-dating it. Although the peak of the Deccan LIP occurs at ca. 66.0–66.5 Ma and >90% eruptions happened at this age [30–32]; however, some lines of evidence support the prolonged period of magmatic pulses between ca. 70.5 and ca. 62 Ma ([33,34] and references therein). The inner and outer tholeiitic basalts are identified in and around the ASACC, and it has been suggested that the Ambadunger carbonatites were emplaced within the Inner tholeiitic basalts rather than the Outer tholeiitic basalts [23]. Further, the Inner tholeiitic basalt is dated by the Ar–Ar method, which placed it at ca. 68.5 ± 0.9 Ma, slightly older than the ages reported for the alkaline complexes [23]. Several examples, including Ambadungar, suggest linkage of carbonatite and alkaline magmatism with the large igneous provinces [35]. This is also well supported by the genetic connection of the Deccan LIP and Ambadungar complex with the Réunion plume; however, both might have had different genetic evolution/sources [35–37]. Therefore, the age suggested by Fosu et al., 2019 [28] looks realistic and suggest emplacement of the ASACC at 65.4 ± 2.5 Ma, slightly younger than the main Deccan LIP event (ca. 66.0–66.5 Ma).

3. Petrography

The garnet grains were studied under transmitted light microscopy (Leica DM750P), back-scattered electron (BSE) imaging and EPMA mapping techniques for their detailed petrographic features. Generally, the studied sample of carbonatite agglomeratic/ brecciated intrusive host are coarse- to medium-grained, brown to dark brown, and contain euhedral/subhedral grains of garnet, embedded in a fine-grained calcitic/ankeritic groundmass. K-feldspar, aegirine-augite, and other lithic fragments are the other phenocrystic/xenocrystic phases present in these samples. Medium-grained calcite grains are also present as independent crystals or occur as clusters. There is no uniform zonation pattern observed in garnet; only their core shows darker color than the rim (see Figure 3). This is also confirmed from the study of BSE images and X-Ray elemental mapping (Figure 4). The observed color shades in the zones of garnets are attributed to the variable concentration of Ti [38–40]; the darker zones have comparatively high-Ti contents than the lighter zones (see Figure 4).

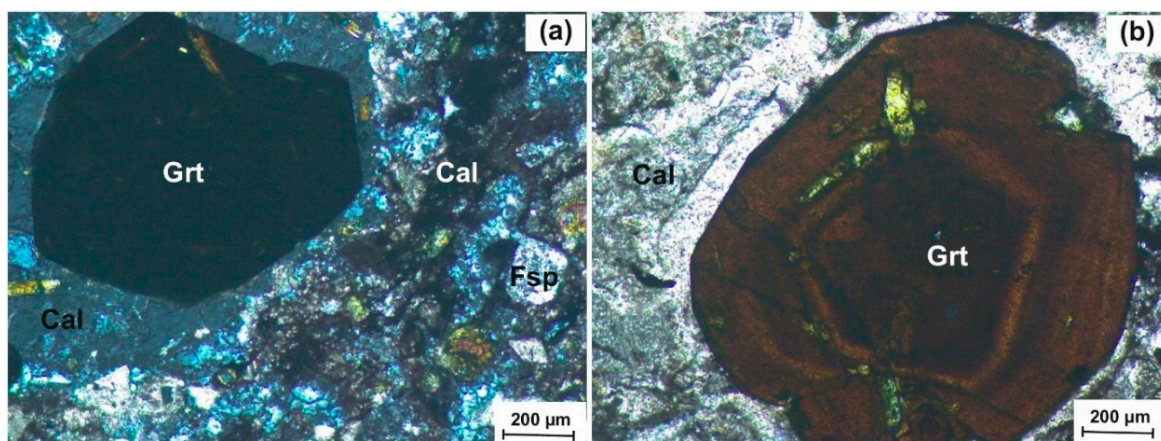


Figure 3. Photomicrographs of a garnet phenocryst in a calcitic groundmass: (a) under XPL (b) under PPL—large euhedral garnet phenocryst showing variation in color. A few K-feldspar grains are also visible. Abbreviations of mineral names are taken from [41].

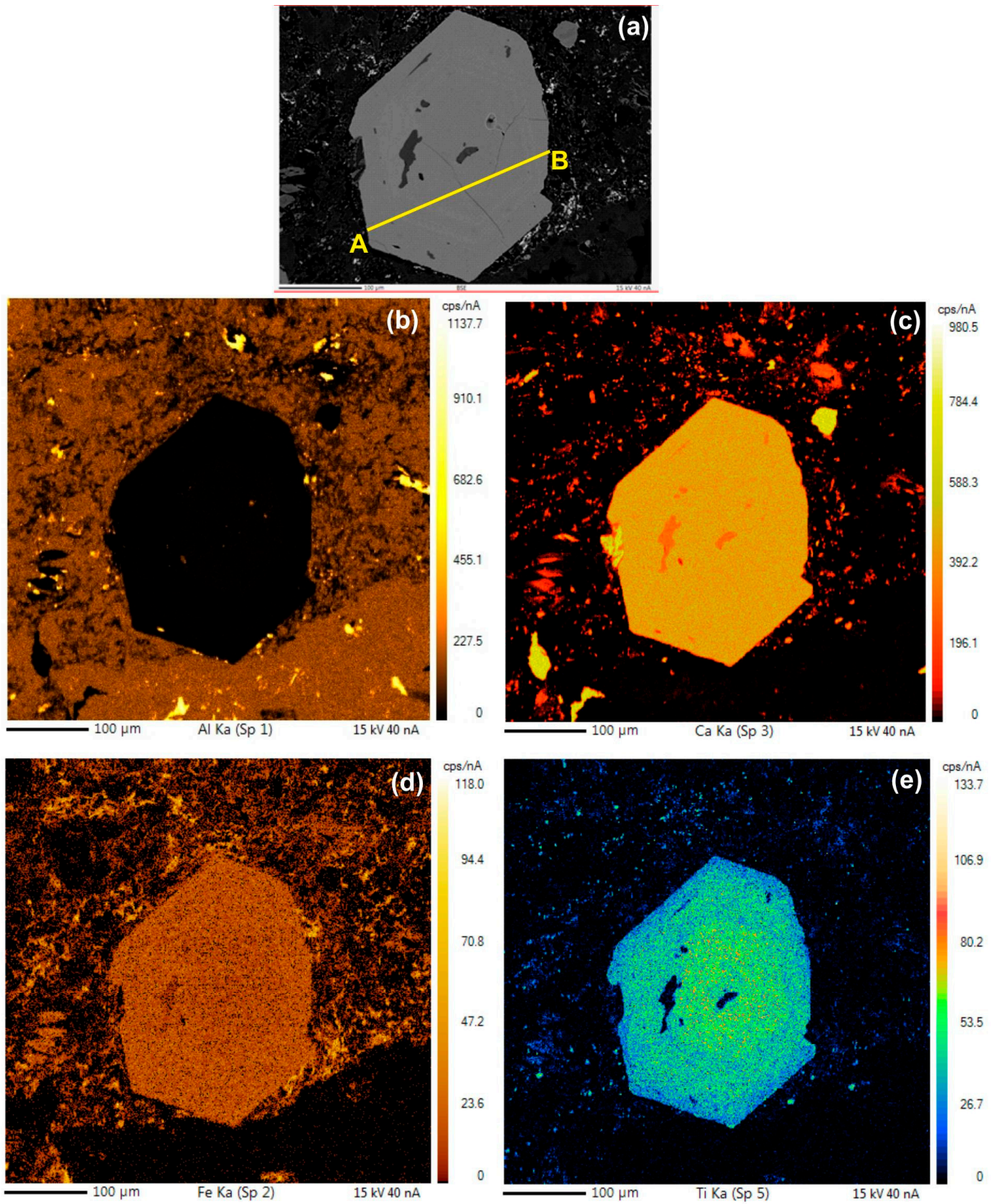


Figure 4. (a) BSE images of garnet grain; no substantial zonation is observed. AB line shown in the figure is used for the EPMA line scan for different oxides as displayed in Figure 5. (b–e) X-Ray Elemental maps for Al, Ca, Fe, and Ti, respectively.

4. Analytical Techniques

Fresh samples (to the extent possible) were collected from the outcrops. The major element composition of the garnets was determined on a CAMECA SX5 electron probe micro analyzer (EPMA) equipped with five wavelength dispersive spectrometers at the Mantle Petrology Lab, Department of Geology, Institute of Science, Banaras Hindu University, Varanasi. An andradite standard is used to verify the positions of crystals (SP1-TAP, SP2-LiF, SP3-LPET, SP4-LTAP, and SP5-PET) prior to measurement. The instrument conditions during calibration and measurement were as follows: acceleration voltage 15kV, beam current of 10 nA, beam diameter <1 μm . Routine calibration, acquisition, quantification, and data processing were carried out using SxSAB version 6.1 and SX-Results software of CAMECA. Mineral chemistry data for garnet is listed in Table 1.

The concentration of trace elements in garnets was measured on a Thermo Fisher Scientific ICAP-Q quadrupole inductively coupled plasma mass spectrometer (ICP-MS) coupled to a New Wave Research 193 ArF excimer laser ablation (LA) system at the Radiogenic Isotope Facility of the Department of Geology and Geophysics, Indian Institute of Technology (IIT), Kharagpur, India. The laser was operated at a repetition rate of 10 Hz, fluence of 5 J/cm², and spot size of 50 μm . The analyses were performed in time-resolved mode, with each analysis consisting of ca. 30 s background measurement with the laser turned off and ca. 40 s peak signal measurement with the laser ablating on the sample. External standardization was done by standard–sample–standard bracketing with ten measurements of the samples bracketed by two analyses of NIST 612 reference glass. The data quality was monitored by ablating the NIST 610 reference glass as unknowns interspersed with the measurements of the samples. The raw data were reduced offline using the GLITTER[®] software version 4.4.4 [42] with Ca as internal standard. The reproducibility estimated from repeat measurements of the NIST 612 and NIST 610 reference glasses is better than 7% for most elements except for Cr (22–25%), Zn (13%), and Ge (13%). The trace element data of the garnets and the NIST reference glasses are listed in Table 2 and Table S1, respectively.

Table 1. Representative EMPA data (wt. %) of garnets from the carbonatite agglomeratic/brecciated intrusive, ASACC. As there are no vacancies in the X and Y site, therefore, the studied garnet is considered as anhydrous.

Oxide (wt. %)	1	2	3	4	5	6	7	8	9	10	11	12	13	14	15
SiO ₂	28.5	28.6	28.73	28.71	28.73	28.69	29.22	29.3	28.66	29.11	28.85	29.26	29.2	29.91	29.58
TiO ₂	12.77	12.8	12.48	12	12.82	12.31	12.27	12.25	12.1	12.2	12.31	13.04	12.75	11.18	11.45
Al ₂ O ₃	2.08	2.24	2.32	2.19	2.17	2.63	2.34	2.33	2.28	2.21	2.21	1.97	1.12	1.39	0.75
Cr ₂ O ₃	0.09	0.10	0.08	0.10	0.08	0.1	0.10	0.07	0.10	0.09	0.10	0.11	0.12	0.11	0.08
V ₂ O ₃	0.57	0.47	0.25	0.38	0.41	0.47	0.38	0.5	0.31	0.54	0.6	0.45	0.66	0.63	0.39
FeO _{tot}	20.95	19.81	20.67	19.65	19.52	20.63	19.63	19.6	21.34	19.84	19.58	19.36	20.95	21.38	22.01
MnO _{tot}	0.29	0.23	0.25	0.34	0.2	0.44	0.42	0.32	0.29	0.38	0.29	0.42	0.34	0.27	0.41
MgO	0.92	0.83	0.8	0.88	0.83	0.77	0.87	0.79	0.91	0.75	0.81	0.72	0.51	0.58	0.57
CaO	33.33	32.8	33.26	32.74	32.54	32.74	32.93	33.14	32.69	32.74	32.72	32.94	32.65	32.95	32.62
Na ₂ O	0.02	0.01	0.03	0.03	0.07	0.06	0.02	0.02	0.05	0.06	0.02	0.07	0.18	0.09	0.10
Total (calc.)	99.51	97.9	98.89	97.02	97.39	98.85	98.18	98.33	98.73	97.92	97.5	98.33	98.48	98.5	97.97
							Recalc. (wt. %)								
final FeO	0.85	1.95	1.16	1.11	2.26	1.38	1.70	1.76	1.12	1.83	1.80	2.48	2.49	1.95	2
final Fe ₂ O ₃	22.33	19.84	21.68	20.61	19.19	21.39	19.92	19.83	22.47	20.02	19.76	18.76	20.52	21.59	22.24
final MnO	0.29	0.23	0.25	0.34	0.2	0.44	0.42	0.32	0.29	0.38	0.29	0.42	0.34	0.27	0.41
final Mn ₂ O ₃	0	0	0	0	0	0	0	0	0	0	0	0	0	0	0
Σ(Recalc.)	101.75	99.89	101.06	99.09	99.32	100.99	100.17	100.31	100.98	99.94	99.48	100.22	100.54	100.67	100.19
							Cations for 12 O atoms								
Mn ²⁺	0.020	0.016	0.018	0.024	0.014	0.031	0.030	0.023	0.020	0.027	0.021	0.030	0.024	0.019	0.030
Mg	0	0.007	0	0	0.011	0.020	0	0	0.033	0	0	0	0	0	0
Ca	2.977	2.974	2.984	2.990	2.964	2.938	2.972	2.986	2.939	2.965	2.977	2.976	2.958	2.970	2.968
Na	0.003	0.002	0.005	0.005	0.011	0.010	0.004	0.004	0.008	0.010	0.004	0.011	0.029	0.014	0.016
ΣX	3.000	3.000	3.007	3.019	3.000	3.000	3.005	3.013	3.000	3.003	3.002	3.017	3.011	3.005	3.014
Ti ⁴⁺	0.801	0.815	0.787	0.769	0.820	0.776	0.777	0.775	0.764	0.776	0.786	0.827	0.811	0.708	0.731
Al ³⁺	0	0	0	0	0	0	0	0	0	0	0	0	0	0	0
Cr ³⁺	0.006	0.006	0.005	0.006	0.005	0.007	0.007	0.004	0.006	0.006	0.006	0.007	0.008	0.007	0.005
Fe ²⁺	0.059	0.138	0.081	0.079	0.160	0.097	0.1197	0.124	0.079	0.129	0.128	0.175	0.176	0.137	0.142
Fe ³⁺	0.981	0.911	1.003	0.987	0.892	1.014	0.955	0.951	1.049	0.955	0.934	0.853	0.886	1.026	1.009
Mn ³⁺	0	0	0	0	0	0	0	0	0	0	0	0	0	0	0
Mg	0.114	0.098	0.100	0.112	0.095	0.075	0.1096	0.099	0.081	0.094	0.102	0.090	0.064	0.073	0.072

Table 1. Cont.

Oxide (wt. %)	1	2	3	4	5	6	7	8	9	10	11	12	13	14	15
V	0.038	0.032	0.017	0.026	0.028	0.031	0.026	0.034	0.021	0.037	0.0409	0.031	0.044	0.042	0.027
ΣY	1.999	2.000	1.993	1.981	2.000	2.000	1.995	1.987	2.000	1.997	1.998	1.983	1.989	1.995	1.986
Si ⁴⁺	2.376	2.421	2.406	2.446	2.443	2.403	2.461	2.464	2.405	2.461	2.45	2.467	2.469	2.519	2.512
Al ³⁺	0.2041	0.223	0.229	0.2198	0.217	0.259	0.232	0.231	0.226	0.220	0.2212	0.196	0.112	0.137	0.075
Fe ³⁺	0.420	0.353	0.364	0.334	0.336	0.335	0.308	0.304	0.370	0.318	0.329	0.337	0.420	0.341	0.412
ΣZ	3	3	3	3	3	3	3	3	3	3	3	3	3	3	3
							End members mol. %								
Andradite	48.41	44.76	50.14	49.38	43.76	48.99	47.5	47.53	50.68	47.24	46.25	42.65	44.29	51.32	50.45
Schorlomite	20.99	17.66	18.18	16.7	16.8	16.74	15.37	15.21	18.48	15.92	16.44	16.85	20.98	17.06	20.63
Schorlomite- Al	10.21	11.16	11.44	10.99	10.86	12.97	11.59	11.57	11.30	11.02	11.06	9.81	5.58	6.88	3.76
Morimotoite	5.94	13.80	8.13	7.92	16.05	9.66	11.97	12.40	7.87	12.91	12.80	17.48	17.57	13.73	14.19
Morimotoite- Mg	11.42	9.82	10.03	11.22	9.48	7.53	10.96	9.91	8.15	9.43	10.25	9.03	6.44	7.32	7.21
Goldmanite	1.90	1.59	0.83	1.30	1.40	1.57	1.29	1.68	1.03	1.84	2.05	1.53	2.23	2.12	1.34
Uvarovite	0.31	0.32	0.25	0.32	0.27	0.33	0.33	0.22	0.32	0.31	0.33	0.36	0.39	0.36	0.27
NaTi Garnet	0.15	0.12	0.26	0.26	0.57	0.5	0.18	0.18	0.4	0.51	0.2	0.57	1.45	0.7	0.8
Calderite	0.65	0.55	0	0	0.47	1.04	0.27	0	0.68	0.5	0.43	0	0	0	0
Khoharite	0	0.13	0	0	0.22	0.59	0	0	1.09	0	0	0	0	0	0
Remainder	0.03	0.09	0.74	1.91	0.14	0.09	0.54	1.31	0	0.30	0.20	1.72	1.07	0.50	1.36
Total (calc.)	100.01	100	100	100	100.02	100.01	100	100.01	100	99.98	100.01	100	100	99.99	100.01
Quality Index	Sup	Sup	Sup	Exc	Sup	Sup	Sup	Exc	Sup	Sup	Sup	Exc	Exc	Sup	Exc

Sup.—Superior; Exc.—Excellent.

Table 2. LA-ICP-MS rare-earth and trace elements data (in ppm) of garnets from the carbonatite agglomeratic/brecciated intrusive, ASACC.

Elements	Rare-Earth Elements															
	1	2	3	4	5	6	7	8	9	10	11	12	13	14	15	16
La	72.1	67.3	52.0	50.8	39.9	52.2	46.8	64.1	47.1	33.1	65.5	51.1	48.6	51.5	49.9	29.35
Ce	379.0	366.0	315.0	283.0	248.0	247.0	276.0	339.0	231.0	202.0	346.0	295.0	275.0	285.0	209.0	162.0
Pr	64.0	63.2	55.0	48.3	46.1	45.5	47.9	61.7	42.3	37.2	63.5	52.0	51.2	46.9	38.8	29.2
Nd	335.0	340.0	295.0	256.0	238.0	234.0	245.0	323.0	225.0	199.0	329.0	281.0	281.0	234.0	198.0	154.4
Sm	87.2	91.6	71.6	60.8	58.1	58.1	64.8	86.3	55.6	51.8	88.1	75.2	75.1	59.9	61.1	45.25
Eu	29.7	32.2	24.3	19.4	19.2	19.5	22.1	29.6	18.6	17.1	31.5	26.8	25.8	20.3	21.0	16.07
Gd	79.9	81.3	61.5	50.9	49.8	49.1	55.61	74.2	46.7	42.7	79.4	68.6	63.0	50.7	50.2	38.52
Tb	12.4	13.5	9.4	7.2	7.1	6.9	8.4	12.0	7.0	6.8	12.8	11.1	10.5	8.19	8.7	6.5
Dy	72.9	78.7	48.2	39.48	39.2	37.4	48.0	70.0	39.1	37.3	75.7	65.4	58.7	47.1	51.7	39.5
Ho	12.9	14.2	8.7	7.1	6.9	6.4	8.2	12.8	6.9	6.6	13.8	12.0	10.6	8.6	9.4	7.0
Er	34.8	38.3	23.3	18.3	18.7	17.1	22.3	33.7	18.7	18.0	36.2	32.3	28.1	24.0	25.6	19.4
Tm	4.5	4.9	3.3	2.5	2.5	2.4	3.1	4.5	2.5	2.5	4.8	4.2	3.7	3.2	3.5	2.6
Yb	31.1	34.5	21.8	16.6	17.0	16.7	20.2	30.2	17.4	16.7	31.5	27.9	24.7	21.3	23.0	17.9
Lu	3.9	4.3	2.8	2.3	2.2	2.3	2.7	3.9	2.4	2.3	4.3	3.7	3.4	2.8	3.1	2.3
∑LREE	967.0	959.9	813.0	718.1	649.3	656.0	702.4	903.8	619.9	539.4	923.5	781.1	757.2	697.1	578.4	435.9
∑HREE	252.5	269.8	179.1	144.3	143.3	138.2	168.6	241.2	140.9	132.9	258.4	225.1	202.7	165.9	175.3	133.8
∑REE	1219.5	1229.7	992.1	862.4	792.6	794.3	871.1	1145.1	760.73	672.3	1181.9	1006.3	959.9	863.0	753.7	569.6
LREE/HREE	3.83	3.56	4.54	4.97	4.53	4.75	4.16	3.75	4.40	4.06	3.57	3.47	3.74	4.20	3.30	3.26
La/Yb	1.6	1.3	1.6	2.1	1.6	2.1	1.6	1.4	1.8	1.3	1.4	1.2	1.3	1.6	1.5	1.1
δEu	1.08	1.14	1.12	1.06	1.09	1.11	1.12	1.13	1.11	1.11	1.15	1.14	1.14	1.13	1.15	1.17

Table 2. Cont.

Rare-Earth Elements																
Elements	1	2	3	4	5	6	7	8	9	10	11	12	13	14	15	16
	Trace Elements															
	1	2	3	4	5	6	7	8	9	10	11	12	13	14	15	16
Sc	15	16	14	12	13	12	14	15	14	14	14	14	13	11	13	10
V	1127	1083	1396	1693	2027	1670	1853	1114	2155	1903	1359	1311	1575	1533	1998	1451
Mn	2694	2616	2822	2629	2822	2660	2705	2369	3558	3197	3062	2777	2757	2693	2749	1863
Co	11	11	8	7	6	7	7	11	7	9	10	9	8	9	9	7
Ni	1	2	2	2	2	2	2	2	1	2	1	2	2	2	2	1
Zn	111	106	81	85	86	64	97	82	136	113	121	111	88	107	106	64
Sr	61	58	49	51	49	54	55	67	178	93	68	61	62	90	59	45
Y	335	365	238	194	194	189	231	335	193	191	362	315	290	244	266	195
Zr	3360	3379	2762	2057	2072	2082	2328	3892	1904	1817	3436	2876	2895	2257	1888	1821
Nb	2282	2134	957	1274	435	964	1196	739	1275	695	1742	1218	718	156	695	282
Hf	62	60	50	38	40	34	41	80	37	37	63	55	56	46	35	40
Ta	78	73	39	33	21	33	48	44	53	28	73	61	36	48	29	15
Th	22	23	14	13	7	11	12	15	8	6	17	13	10	12	7	5
U	22	21	17	14	10	14	16	16	13	10	19	14	12	14	11	6

5. Results

Major and Trace Element Geochemistry

The garnet formula is normalized to 12 oxygen and 8 cations and calculated using the Excel-based program [43]. According to the quality index [43], most of the analyses are superior, and some are excellent. The re-calculated totals of the oxides are between 99.09 wt. % and 101.8 wt. %, which confirms the excellent quality of the EPMA data. The compositional variation in terms of the concentration of the major element oxides is as follows: CaO (32.54–33.33), Al₂O₃ (0.74–2.63), Fe₂O₃ (19.36–22.73), Cr₂O₃ (0.07–0.13). The characteristic compositional feature of these garnets is the enrichment in TiO₂, which varies between 10.03 wt. % and 13.04 wt. %. The garnets have variable Fe, Al, and Ti (apfu), resulting in the presence of several end members. Mostly, the compositional variations can be explained through the andradite (42.65–57.25%), schorlomite (22.01–31.01%) and morimotoite (15.64–26.51%) components. The hypothetical end members schorlomite-Al, morimotoite-Mg (see Table 1) are also expressed as schorlomite and morimotoite, respectively. As no significant MgO and MnO are measured, grossular and spessartite end members are absent. The EPMA line scans along A–B for the phenocryst shown in Figure 5 do not reveal any significant compositional zoning in Ca, Si, and Al; however, Ti and Fe show some variations. X-ray element maps of Fe, Ca, Al, and Ti reveal minor variation in Ti, with concentrations slightly elevated in the core regions. Most other elements do not display any significant compositional variation (see Figure 4). The relatively weak intensity of the elemental variation makes it hard to interpret any zonation pattern.

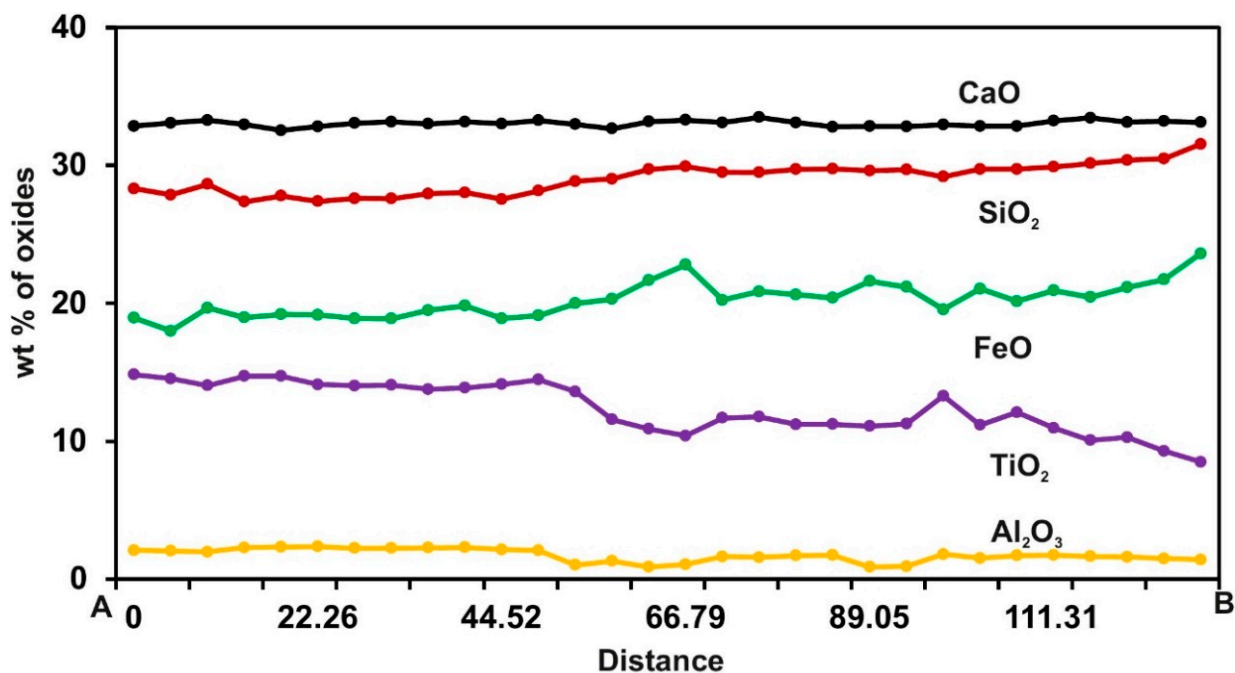


Figure 5. EPMA line scans along the line A–B (as shown in Figure 4a) for various oxides in the studied garnet grain.

A total of 16 LA-ICP-MS spot analyses were carried out on garnet grains. This includes both core and rim regions of grains. The studied garnets show similar chondrite normalized REE patterns with a slight positive anomaly at Europium ($\text{Eu}/\text{Eu}^* = 1.06$ to 1.17). The REE patterns are characterized by enrichment of the LREE and MREE (Ce to Dy) relative to La and the HREE, giving it a convex upward pattern (Figure 6a). The total REE concentration varies between 570 and 1230 ppm. The abundance of MREE (middle REE) and LREE (LREE = 436–967, average 731 ppm) is relatively higher compared to the HREE (HREE = 133–270 ppm, average 186 ppm). The $\sum\text{LREE}/\sum\text{HREE}$ ratio varies between 3.26 and 4.97, while the La_N/Yb_N varies between 1.11 and 2.11. The relative depletion of La relative to the other LREE is a noteworthy feature of the REE patterns. In a multi-

element plot, all analyses show strong enrichment of U (6–22 ppm), Nb (282–2283 ppm), Ta (15–78 ppm), Zr (1816–3892 ppm), Hf (34–80 ppm), and V (1083–2155 ppm) and depletion of La (29–72 ppm) and Sr (45–178 ppm) (Figure 6b).

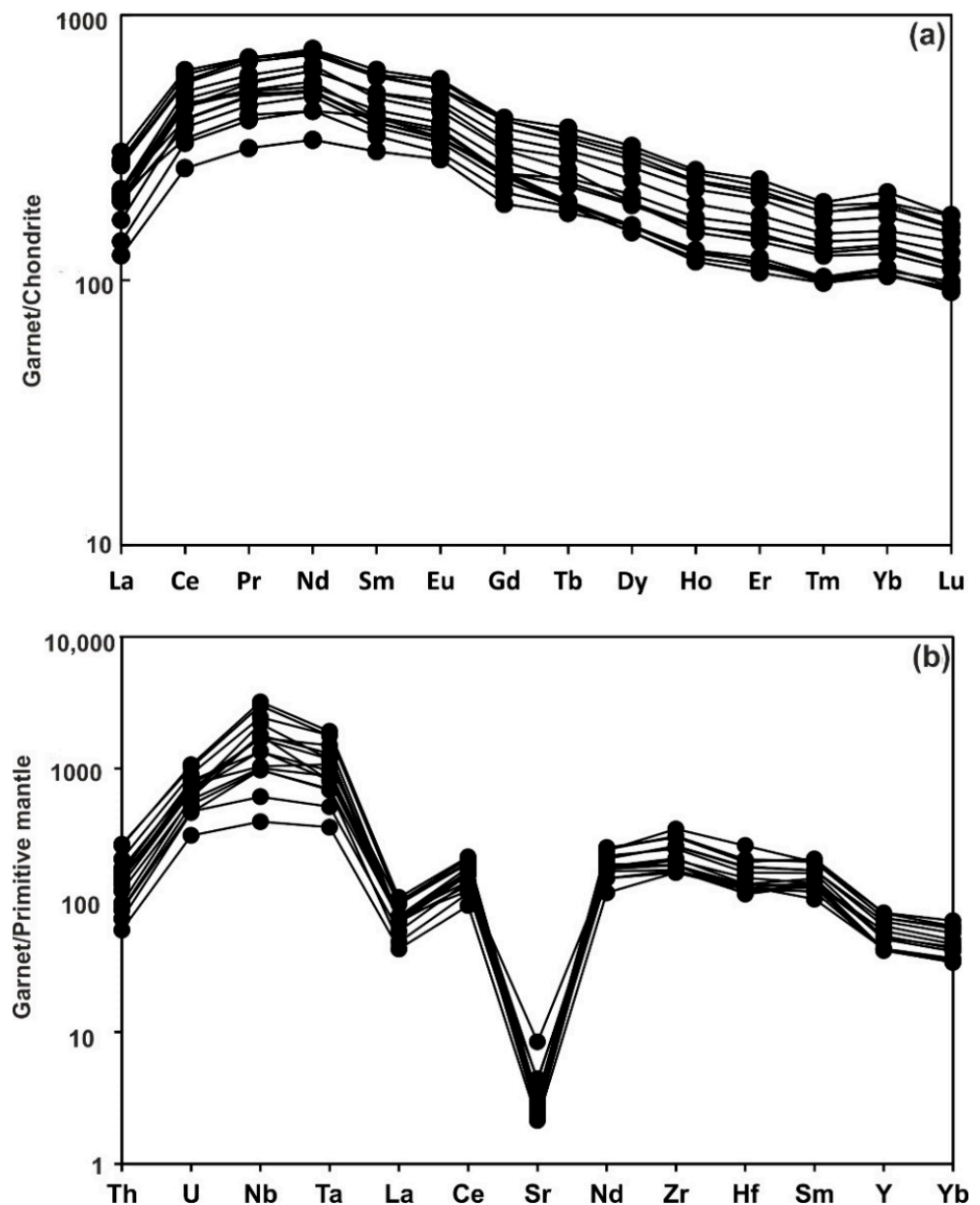


Figure 6. (a) Chondrite-normalized REE patterns of studied garnet. (b) Primitive mantle-normalized multi-element diagram of the studied garnet. Chondrite and primitive mantle values are taken from [44,45], respectively.

6. Discussion

6.1. Site Occupancies of Ti in Garnet and Its Classification

Although a number of studies have been carried out on different varieties of Ti-rich garnet, the preferential site-specific substitution of Ti and Fe is not yet resolved [2]. Several site-specific substitutions involving combinations of some or all the cations Fe^{2+} , Fe^{3+} , Al, Ti^{4+} , and Ti^{3+} in octahedral, tetrahedral, and dodecahedral sites have been suggested [46]. In the present study, we have followed the recommendations of Locock [43]. As it is difficult to determine the distribution of a given element among three sites in the absence of spectroscopic or site-refinement data, each element of a given valence state is limited

to either one or two sites. In the stoichiometric calculations, Mg, Al, Si, Ti, V, Cr, Mn³⁺, Fe²⁺, and Fe³⁺ are assigned at the octahedral (Y) site, and Al, Si, and Fe³⁺ are assigned at the tetrahedral (Z) site (see Table 1). Initially, all Si were assigned to the tetrahedral site; if necessary, Al³⁺ and Fe³⁺ were used to fill the remainder of the tetrahedral site to make it up to 3 apfu. In the octahedral site (Y), any Si in excess of 3 apfu, after allotment in the Z site is assigned. The Ti⁴⁺ content varies from 0.64 to 0.82 apfu at the Y site, whereas the Si content ranges from 2.37 to 2.55 at the Z site in the studied garnet. The Y-site Ti (apfu), when plotted against Z-site Si (apfu) shows a strong negative correlation (Figure 7), which suggests that Ti substitutes for Si. As the garnet compositions plot close to the 2Ti:1Si (see the dotted line in Figure 7), the exchange of Si for Ti was not one-to-one [47]. This is balanced by adding Fe²⁺ and Fe³⁺ at the Y site and some Fe³⁺ at the Z site.

As the studied garnets do not contain pyrope, grossular, and spessartine end members, therefore, in the spessartine + pyrope-Ti-andradite-grossular compositional space, they plot near Ti-andradite composition (not shown). In the literature, Ti-andradite, schorlomite and melanite are three frequently used nomenclature of Ti-rich garnet. The principles for distinguishing schorlomite from Ti-andradite have been suggested by Chakhmouradian and McCammon, 2005 [48]. It is suggested that in the case of schorlomite, ^YTi > ^YFe³⁺ [3,49] and TiO₂ is >15 wt. % [50]. Ti-rich andradites are also classified into melanite and schorlomite depending on whether Fe³⁺ or Ti predominates in the octahedral site, placing the limit approximately at 15 wt. % TiO₂ [3]. According to this classification scheme, the studied Ti-rich andradites are classified as melanite as it contains a maximum of 13.04 wt. %, of TiO₂.

The Ti-rich garnets of Ambadungar were earlier classified as melanite [20]; however, this is not consistent with the recommended classification scheme. According to the International Mineralogical Association–The Commission on New Minerals, Nomenclature and Classification (IMA-CNMNC), melanite is considered as a varietal name, and schorlomite and morimotoite are the two Ti-rich garnet species that are currently accepted [2]. While the studied garnet contains andradite, schorlomite and morimotoite end members (see Table 1), therefore, it can be a member of this series.

6.2. Genesis of Garnet: Primary vs. Metasomatic

Generally, Ti-rich garnets have been reported to occur in a wide variety of parageneses, from primary igneous to deuteric and hydrothermal, as well as low- to high-grade metamorphic rocks [3,40,51]. They constitute a ubiquitous phase in many volcanic and plutonic alkaline igneous rocks and carbonatites [3,40]. Although generally observed as a primary phase in many alkaline rocks, garnets also occur as interstitial or irregular grains in the groundmass formed by metasomatic reactions of earlier formed phases and late-stage fluid [52]. Due to similar chemical and mineralogical composition, the discrimination between metasomatic and primary magmatic Ca-rich garnet is always problematic [9]. Therefore, major and trace element characteristics have been investigated to confirm the genesis of the studied garnet.

Based on major element geochemistry and textural evidence of Ti-rich garnets from the ASACC, the possibility of their primary magmatic nature is doubtful [20]. The high Ti content of these garnets (up to ~14 wt. %) and correspondingly not having any other Ti bearing phases makes a critical question on the primary magmatic origin of these garnets. An analogous case study is reported from the Sung Valley, where garnets from the ijolite sample show similar TiO₂ contents [53] (see Figure 8). They have observed a reaction rim of titanite and garnet on perovskite, and based on this, a crystallization sequence perovskite–titanite–Ti-garnet has been defined. These observations attest to a change in the chemical composition of coexisting silicate melts and also confirm a primary magmatic origin of garnet. On the contrary, the studied rock does not show any such crystallization sequence and textural evidence. Therefore, based on the absence of textural evidence, the primary magmatic origin of studied garnets is discarded. Moreover, titanium enrichment in

the rock types of the Ambadungar complex was earlier reported in several studies [54–56] in which authors report the presence of Ti-rich pyrochlore and ilmenite.

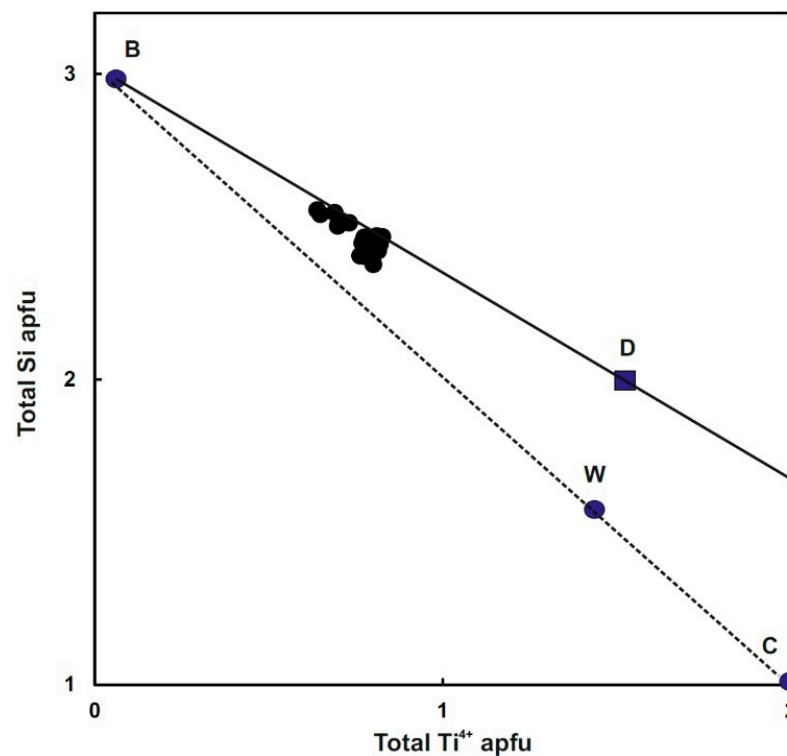


Figure 7. Variation of Si content at the Z site with Ti^{4+} content at the Y site [47]. Point W represents a synthetic sample [57], and point C represents the position where $Ti = 2$ and $Si = 1$ apfu. Point D represents the composition midway between schorlomite and morimotoite.

In general, the studied garnet is enriched in LREE (average 731 ppm) and is relatively depleted in HREE (average 186 ppm). The LREE/HREE ratio varies from 3.21 to 4.89, whereas La_N/Yb_N varies from 1.11 to 2.11. By and large, LREE-enriched and HREE-depleted REE pattern (see Figure 6a) is displayed by andradite–grossular garnets found in skarn deposits [6,8,58–61]. On the other hand, the HREE-enriched and LREE-depleted REE pattern is mainly displayed by Al-rich garnets (pyrope, almandine, spessartine, and grossular) from metamorphic and magmatic systems [5,62–71]. The observed LREE enriched pattern of the studied garnets (Figure 6a) is similar to the REE pattern of skarn deposit, which attests to the active role of metasomatic processes involving hydrothermal fluids. Our observation of LREE enrichment in garnet is consistent with the earlier studies [56,72]; it is suggested that hydrothermal activity is the primary factor accountable for the significant LREE mineralization in the Ambadungar complex.

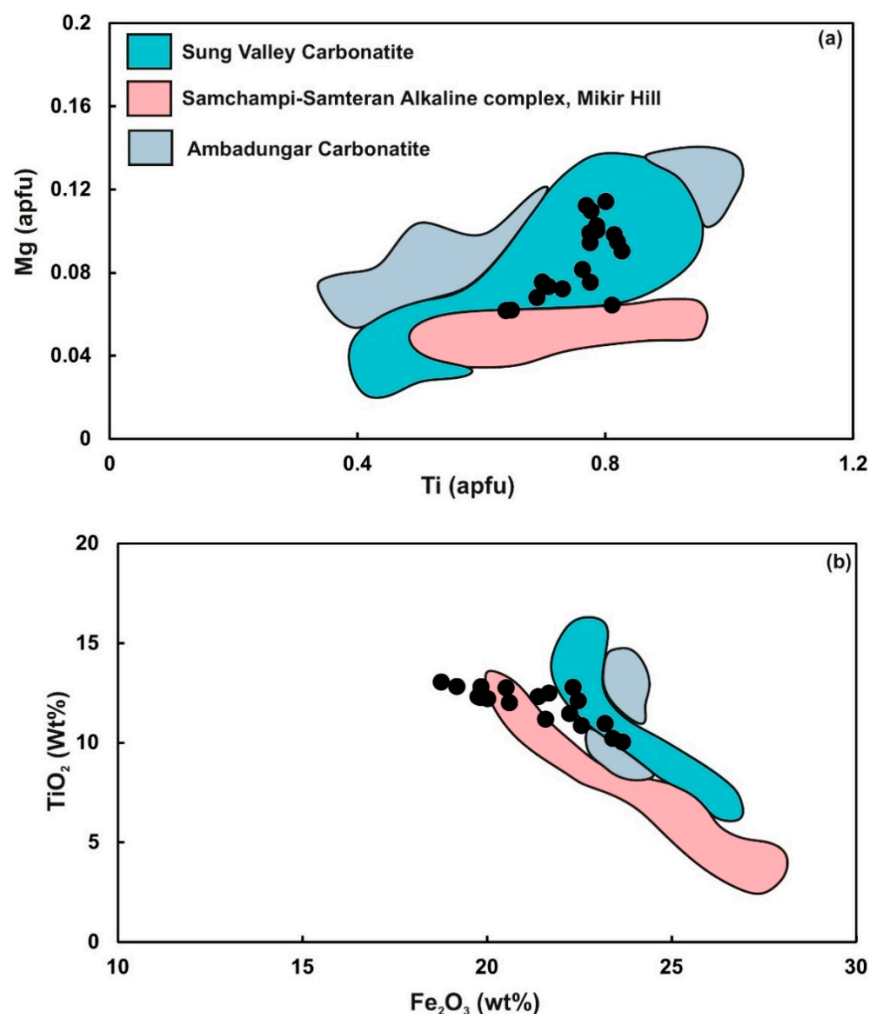


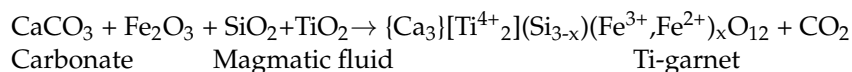
Figure 8. (a) TiO_2 versus Fe_2O_3 , and (b) Mg (apfu) versus Ti (apfu) diagrams for the studied garnet. Compositional range of garnets from Sung Valley carbonatites [53], Samchampi-Samteran [73], Ambadungar [20] are also shown for comparison.

One of the most intriguing features of the studied garnets is the depletion of La and enrichment of Ce-Pr-Nd, showing a convex upward pattern. This pattern is similar to a typical M-type first tetrad (La, Ce, Pr, and Nd). The lanthanide tetrad effect (M or W type), first reported on REE pattern of natural samples [74] that produces four separate curves (consisting of La–Ce–Pr–Nd, Pm–Sm–Eu–Gd, Gd–Tb–Dy–Ho, and Er–Tm–Yb–Lu). Usually, the maximum M-type tetrad effect between La and Nd is related to the character of REE partitioning between fluoride and silicate melts and F- and Cl-rich magmatic fluids [75]. Therefore, the presence of M-type tetrad in the studied garnets is suggestive of crystallization under fluid-rich conditions.

In the calcium garnet series, V^{3+} substitutes for Al^{3+} and Fe^{3+} ; therefore, vanadium is usually present in the garnet in trace quantity. V_2O_3 is a rare component of calcium bearing garnet [76]. Vanadium-rich grossular containing 4.52 wt. % V_2O_3 (supposed to be very high) has also been reported [77]. Vanadium is not unusual in carbonatites as well; therefore, it is suggested that V can be accommodated in aegirine and magnetite [78]. Vanadium contents in the studied garnet are high, which varies from 1.08 to 2.15 wt. % (see Table 2). The high content of vanadium has also been noticed from the sövites of Ambadungar, where vanadium is present in wakefieldite and forms separate phase vanadinite [56]. Magnetite and ilmenite, reported in several rock types of Ambadungar, could be the primary source of vanadium. Hydrothermal fluid has induced its alteration, making the mobilization of V (along with Ti) from greater depth and precipitating closer to the surface. Our observation

is consistent with the proposal of Magna et al., 2020 [56], in which they have explained the vanadium enrichment in sövite due to the role of hydrothermal fluid. Further, the studied garnet grains also show a significantly high content of Nb, with the highest value of 2283 ppm. Moreover, the high Nb content has also been reported from the several varieties of carbonatites of Ambadungar. The sövite and ankeritic varieties of carbonatite show Nb variation from 25 to ~3000 ppm; with the highest content of ~5000 ppm [14,56]. In these rocks (mostly sövites), pyrochlore is the primary Nb-bearing phase constituting up to 50 modal %, and it shows a wide range of crystallization conditions starting from the cumulate level to the late carbonatite phase [55]. Therefore, pyrochlore has been suggested to the source for Nb, and it is released during its interaction with the hydrothermal fluid.

Based on textural evidence, REE pattern and the presence of abnormally high content of Ti, Nb, and V, the reaction between hydrothermal fluid and early formed minerals is suggested for the genesis of garnet in the Ambadungar complex. Further, the geochemical data suggest that the hydrothermal fluid must be enriched in Fe, Si, LREE, Nb, V, and Ti content. Therefore, the following reaction can be postulated for the growth of hydrothermal garnet:



Magnetite, ilmenite, and pyrochlore present in different varieties of carbonatites in the Ambadungar complex could be the primary source for these elements.

6.3. Nature of Hydrothermal Fluid

A broader understanding of factors controlling REE mobility during fluid-rock interaction is required to interpret the REE patterns [79]. The pH of hydrothermal fluid primarily controls the REE fractionation; oxygen fugacity and the presence of ligand have also substantial influence [79]. Under nearly mildly acidic pH and at higher temperatures, the LREE are more efficiently transported as their complexes have higher stability constants [80]. The higher LREE concentrations of the garnet suggest that the garnet growth must have occurred from a relatively high-T LREE-enriched hydrothermal fluid. The fluid was enriched in the LREE relative to the HREE and had positive or variable Eu anomaly, which is also the general characteristics of common magmatic-hydrothermal fluids [4,79]. On the other hand, under neutral pH, the REE pattern becomes reversed with a negative or no Eu anomaly. The observed LREE enriched REE pattern with moderately positive Eu anomaly of the studied garnet provides compelling evidence for an acidic pH of the hydrothermal fluid.

As the REE complexes of chloride (Cl^-) and sulfate (SO_4^{2-}) have high stability, therefore, these are considered to be the primary ligands for transporting REE. [81,82]. Moreover, Cl^- is considered to be the carrier of Eu^{2+} ; therefore, the Eu anomaly is strongly controlled by its presence [4]. The negative Eu anomalies might be explained by the absence of Cl^- [83]. As the studied garnets do not show prominent positive Eu anomaly, therefore, Cl^- is not considered as a primary ligand in the hydrothermal fluid. Moreover, a very negligible amount of Cl^- (below the detection limit) in the altered apatite from the Ambadungar carbonatite is reported by Fosu et al., 2018 [28]. Therefore, Cl^- was unlikely to have been present in any significant amount in the hydrothermal fluid. The REEs were most likely transported as sulfate complexes in F-rich fluids.

The role of hydrothermal activity in ASACC and nearby alkaline complexes has been reported in several studies. The different rock types of the Ambadungar complex were metasomatized due to hydrothermal fluid, which was released during the last phase of carbonatite magmatism [55]. Similarly, Viladkar and Wimmenauer, 1992 [54] and Viladkar, 1996 [19] have observed that hydrothermal fluids in Ambadungar were rich in F, Si, Fe, Sr, U, Th, and Ba. Based on the presence of wakefieldite and vanadinite in sövites of the Ambadungar complex, the role of hydrothermal solutions has been proposed by [56]. These authors have also suggested a high amount of vanadium in the hydrothermal solutions towards the end of the carbonatite magma activity. The famous fluorite deposit and LREE

mineralization in Ambadungar can be attributed due to the effect of low-salinity (0.8–1.8 wt. % equivalent NaCl), low-temperature (100–150 °C) CO₂-bearing aqueous fluids [72,84]. The unusual oxygen isotope compositions of sövites at Ambadungar could be due to the activity of low-temperature hydrothermal activity [85–88]. The role of high activity of OH[−], (SO₄)^{2−}, Al, and Si in the fluid are reported from the hydrothermal REE mineralization in the Ambadungar carbonatite complex as well [72]. Similarly, based on the noble gas composition of carbonatites from ASACC [89], the role of hydrothermal fluid is suggested. Therefore, the hydrothermal overprinting of the different rock types of the ASACC complex is recommended.

7. Conclusions

Based on the new major, trace, and rare-earth element geochemistry of garnets from the Ambadungar-Saidivasan alkaline carbonatite complex, the following conclusions are drawn:

- The garnets are rich in TiO₂ and characterized by andradite, schorlomite, and morimotoite end members in decreasing order.
- The garnets do not display any distinct chemical zonation; only minor variations in Ti content are observed.
- Based on textural evidence, LREE enriched REE pattern with M-type first tetrad and the presence of abnormally high content of Ti, Nb, and V, the role of metasomatic reactions between earlier formed minerals and hydrothermal fluid enriched in Fe, Si, LREE, U, Nb, V, and Ti content is suggested for the genesis of garnets.
- Magnetite, ilmenite, and pyrochlore present in different varieties of carbonatites in the Ambadungar-Saidivasan complex could be the primary source for these elements released during interaction with hydrothermal fluids. The hydrothermal fluid is moderately acidic pH having fluorine and sulfate as primary ligands.

Supplementary Materials: The following are available online at <https://www.mdpi.com/article/10.3390/min11070756/s1>, Table S1: Analyses of NIST 612 reference glass. External standardization was done by standard-sample-standard bracketing with ten measurements of the samples bracketed by two analyses of NIST 612 reference glass.

Author Contributions: Conceptualization, R.K.S. and A.K.S.; methodology, A.K.S. and D.U.; investigation, R.K.S., A.K.S. and D.U.; data curation, A.K.S. and D.U.; writing—original draft preparation, A.K.S.; writing—review and editing, R.K.S. and D.U.; supervision, R.K.S.; project administration, A.K.S.; funding acquisition, A.K.S. and R.K.S. All authors have read and agreed to the published version of the manuscript.

Funding: This research was funded by the Ministry of Mines, Government of India, grant Number Met 4-14/11/19 to A.K.S. and the DST-SERB, New Delhi, grant Number IR/S4/ESF-18/2011 to R.K.S.

Data Availability Statement: The data is presented directly in the study.

Acknowledgments: R.K.S. and A.K.S. thank Deepak Kumar for his help during EPMA analysis. The authors are thankful to Vincenza Guarino, Guest Editor of this ‘Minerals’ special issue, for inviting us for the contribution. The authors are also grateful to the Head of the Department of Geology, Banaras Hindu University, and the Head, Department of Geology and Geophysics, IIT-Kharagpur, for extending all necessary facilities during this work. The two anonymous reviewers have been thanked for their insightful and timely review.

Conflicts of Interest: The authors declare no conflict of interest.

References

1. Deer, W.A.; Howie, R.A.; Zussman, J. *Rock Forming Minerals: Orthosilicates*; Geological Society: London, UK, 1997; p. 918.
2. Grew, E.S.; Locock, A.J.; Mills, S.J.; Galuskina, I.O.; Galuskin, E.V.; Hålenius, U. Nomenclature of the garnet supergroup. *Am. Mineral.* **2013**, *98*, 785–811. [[CrossRef](#)]
3. Deer, W.A.; Howie, R.A.; Zussman, J. *Rock-Forming Minerals, IA: Orthosilicates*; Longman: New York, NY, USA, 1982.

4. Gaspar, M.; Knaack, C.; Meinert, L.D.; Moretti, R. REE in skarn systems: A LA-ICP-MS study of garnets from the Crown Jewel gold deposit. *Geochim. Cosmochim. Acta* **2008**, *72*, 185–205. [[CrossRef](#)]
5. Hickmott, D.D.; Spear, F.S. Major-and trace-element zoning in garnets from calcareous pelites in the NW Shelburne Falls Quadrangle, Massachusetts: Garnet growth histories in retrograded rocks. *J. Petrol.* **1992**, *33*, 965–1005. [[CrossRef](#)]
6. Jamtveit, B.; Hervig, R.L. Constraints on transport and kinetics in hydrothermal systems from zoned garnet crystals. *Science* **1994**, *263*, 505–508. [[CrossRef](#)] [[PubMed](#)]
7. Chernoff, C.B.; Carlson, W.D. Trace element zoning as a record of chemical disequilibrium during garnet growth. *Geology* **1999**, *27*, 555–558. [[CrossRef](#)]
8. Smith, M.P.; Henderson, P.; Jeffries, T.E.R.; Long, J.; Williams, C.T. The rare earth elements and uranium in garnets from the Beinn and Dubhaich Aureole, Skye, Scotland, UK: Constraints on processes in a dynamic hydrothermal system. *J. Petrol.* **2004**, *45*, 457–484. [[CrossRef](#)]
9. Scheibner, B.; Wörner, G.; Civetta, L.; Stosch, H.G.; Simon, K.; Kronz, A. Rare earth element fractionation in magmatic Ca-rich garnets. *Contr. Mineral. Petrol.* **2007**, *154*, 55–74. [[CrossRef](#)]
10. Sukheswala, R.N.; Borges, S.M. The carbonatite-injected sandstones of Siriwasan, Chhota Udaipur, Gujarat. *Indian J. Earth Sci.* **1975**, *2*, 1–10.
11. Viladkar, S.G. The carbonatites of Amba Dongar, Gujarat, India. *Bull. Geol. Soc. Finl.* **1981**, *53*, 17–28. [[CrossRef](#)]
12. Gwalani, L.G.; Rock, N.M.S.; Chang, W.J.; Fernandez, S.; Allegre, C.J.; Prinzhofer, A. Alkaline rocks and carbonatites of Amba Dongar and adjacent areas, Deccan Igneous Province, Gujarat, India: 1. Geology, Petrography and Petrochemistry. *Mineral. Petrol.* **1993**, *47*, 219–253. [[CrossRef](#)]
13. Srivastava, R.K.; Hall, R.P. Tectonic setting of Indian carbonatites. In *Magmatism in Relation to Diverse Tectonic Settings*; Oxford & IBH Publishers: New Delhi, India, 1995; pp. 135–154.
14. Srivastava, R.K. Petrology, geochemistry and genesis of rift-related carbonatites of Ambadungar, India. *Mineral. Petrol.* **1997**, *61*, 47–66. [[CrossRef](#)]
15. Viladkar, S.G.; Gittins, J. Trace elements and REE geochemistry of Siriwasan carbonatites. *J. Geol. Soc. India* **2016**, *87*, 709–715. [[CrossRef](#)]
16. Krishnamurthy, P. Carbonatites of India. *J. Geol. Soc. India* **2019**, *94*, 117–138. [[CrossRef](#)]
17. Srivastava, R.K. Petrology, Petrochemistry and Genesis of the alkaline rocks associated with the Ambdungar carbonatite complex, Baroda district, Gujarat, India. *J. Geol. Soc. India* **1994**, *43*, 23–39.
18. Sukheswala, R.N.; Udas, G.R. Note on the carbonatite of Amba Dongar (Gujarat State) and its economic potentialities. *Sci. Cult.* **1963**, *29*, 563–568.
19. Viladkar, S.G. *Geology of the Carbonatite-Alkalic Diatreme of Amba Dongar, Gujarat*; Gujarat Mineral Development Corporation: Ahmedabad, India, 1996; p. 74.
20. Gwalani, L.G.; Rock, N.M.S.; Ramasamy, R.; Griffin, B.J.; Mulai, B.P. Complexly zoned Ti-rich melanite-schorlomite garnets from Ambadungar carbonatite-alkalic complex, Deccan igneous province, Gujarat State, western India. *J. Asian Earth Sci.* **2000**, *18*, 163–176. [[CrossRef](#)]
21. Krishnamurthy, P. Carbonatites of India. *Explor. Res. At. Miner.* **1988**, *1*, 81–115. [[CrossRef](#)]
22. Karkare, S.G.; Srivastava, R.K. Regional dyke swarms related to the Deccan Trap alkaline province, India. In *Mafic Dykes and Emplacement Mechanisms*; Parker, A.J., Rickwood, P.C., Tucker, D.I.-I., Eds.; Balkema: Rotterdam, The Netherlands, 1990; pp. 335–347.
23. Ray, J.S.; Pande, K.; Pattanayak, S.K. Evolution of the Amba Dongar Carbonatite Complex: Constraints from ⁴⁰Ar-³⁹Ar chronologies of the Inner Basalt and an alkaline plug. *Intl. Geol. Rev.* **2003**, *45*, 857–862. [[CrossRef](#)]
24. Ray, J.S.; Shukla, P.N. Trace element geochemistry of Amba Dongar carbonatite complex, India: Evidence for fractional crystallization and silicate-carbonate melt immiscibility. *J. Earth Syst. Sci.* **2004**, *113*, 519–531. [[CrossRef](#)]
25. Viladkar, S.G. Ferro-carbonatites in the Amba Dongar Diatreme, Gujarat, India. *J. Geol. Soc. India* **2018**, *92*, 141–144. [[CrossRef](#)]
26. Ray, J.S.; Pande, K. Carbonatite-alkaline magmatism associated with continental flood basalts at stratigraphic boundaries: Cause for mass extinctions. *Geoph. Res. Lett.* **1999**, *26*, 1917–1920. [[CrossRef](#)]
27. Ray, J.S.; Pande, K.; Venkatesan, T.R. Emplacement of Amba Dongar carbonatite-alkaline complex at Cretaceous/Tertiary boundary: Evidence from Ar⁴⁰-Ar³⁹ chronology. *Proc. Indian Acad. Sci. Earth Planet. Sci.* **2000**, *109*, 39–47.
28. Fosu, B.R.; Ghosh, P.; Chew, D.M.; Viladkar, S.G. Composition and U-Pb ages of apatite in the Amba Dongar carbonatite-alkaline complex, India. *Geol. J.* **2019**, *54*, 3438–3454. [[CrossRef](#)]
29. Basu, A.R.; Renne, P.R.; DasGupta, D.K.; Teichmann, F.; Poreda, R.J. Early and late alkali igneous pulses and a high-3 He plume origin for the Deccan flood basalts. *Science* **1993**, *261*, 902–906. [[CrossRef](#)]
30. Chenet, A.L.; Courtillot, V.; Fluteau, F.; Gérard, M.; Quidelleur, X.; Khadri, S.F.R.; Subbarao, K.V.; Thordarson, T. Determination of rapid Deccan eruptions across the Cretaceous-Tertiary boundary using paleomagnetic secular variation: 2. Constraints from analysis of eight new sections and synthesis for a 3500-m-thick composite section. *J. Geophys. Res.* **2009**, *114*, B06103. [[CrossRef](#)]
31. Schoene, B.; Eddy, M.P.; Samperton, K.M.; Keller, C.B.; Keller, G.; Adatte, T.; Khadri, S.F.R. U-Pb constraints on pulsed eruption of the Deccan Traps across the end-Cretaceous mass extinction. *Science* **2019**, *363*, 862–866. [[CrossRef](#)] [[PubMed](#)]
32. Sprain, C.J.; Renne, P.R.; Vanderkluyzen, L.; Pande, K.; Self, S.; Mittal, T. The eruptive tempo of Deccan volcanism in relation to the Cretaceous-Paleogene boundary. *Science* **2019**, *363*, 866–870. [[CrossRef](#)] [[PubMed](#)]

33. Pande, K. Age and duration of the Deccan Traps, India: A review of radiometric and paleomagnetic constraints. *J. Earth Syst. Sci.* **2002**, *111*, 115. [[CrossRef](#)]
34. Srivastava, R.K.; Wang, F.; Shi, W. Substantiation of Réunion plume induced prolonged magmatic pulses (ca. 70.5–65.5 Ma) of the Deccan LIP in the Chhotanagpur Gneissic Complex, eastern India: Constraints from $^{40}\text{Ar}/^{39}\text{Ar}$ geochronology. *J. Earth Syst. Sci.* **2020**, *129*, 1–10. [[CrossRef](#)]
35. Ernst, R.E.; Bell, K. Large igneous provinces (LIPs) and carbonatites. *Mineral. Petrol.* **2010**, *98*, 55–76. [[CrossRef](#)]
36. Simmoneti, A.; Bell, K.; Viladkar, S.G. Isotopic data from the Amba Dongar carbonatite complex, West-Central India: Evidence for an enriched mantle source. *Chem. Geol.* **1995**, *122*, 185–198. [[CrossRef](#)]
37. Simonetti, A.; Goldstein, S.L.; Schmidberger, S.S.; Viladkar, S.G. Geochemical and Nd, Pb, and Sr isotope data from Deccan alkaline complexes—Inferences for mantle sources and plume-lithosphere interaction. *J. Petrol.* **1998**, *39*, 1847–1864. [[CrossRef](#)]
38. Gomes, C.D.B. Electron microprobe analysis of zoned melanites. *Am. Mineral.* **1969**, *54*, 1654–1661.
39. Pearce, T.H. The analcite-bearing volcanic rocks of the Crownsnest Formation, Alberta. *Can. J. Earth Sci.* **1970**, *7*, 46–66. [[CrossRef](#)]
40. Dingwell, D.B.; Brearley, M. Mineral chemistry of igneous melanite garnets from analcite-bearing volcanic rocks, Alberta, Canada. *Contr. Mineral. Petrol.* **1985**, *90*, 29–35. [[CrossRef](#)]
41. Whitney, D.L.; Evans, B.W. Abbreviations for names of rock-forming minerals. *Am. Mineral.* **2010**, *95*, 185–187. [[CrossRef](#)]
42. Griffin, W.L.; Powell, W.J.; Pearson, N.J.; O'Reilly, S.Y. GLITTER: Data reduction software for laser ablation ICP-MS. In *Laser Ablation ICP-MS in the Earth Sciences: Current Practices and Outstanding Issues*; Short Course Series; Sylvester, P., Ed.; Mineralogical Association of Canada: Québec, QC, Canada, 2008; Volume 40, pp. 307–311.
43. Locock, A.J. An Excel spreadsheet to recast analyses of garnet into end-member components, and a synopsis of the crystal chemistry of natural silicate garnets. *Comput. Geosci.* **2008**, *34*, 1769–1780. [[CrossRef](#)]
44. Antao, S.M.; Mohib, S.; Zaman, M.; Marr, R.A. Ti-rich Andradites: Chemistry, structure, multi-phases, optical anisotropy, and oscillatory zoning. *Canad. Mineral.* **2015**, *53*, 133–158. [[CrossRef](#)]
45. McDonough, W.F.; Sun, S.S. The composition of the Earth. *Chem. Geol.* **1995**, *120*, 223–253. [[CrossRef](#)]
46. Brod, J.A.; Junqueira-Brod, T.C.; Gaspar, J.C.; Gibson, S.A.; Thompson, R.N. Ti-rich and Ti-poor garnet from the Tapira Carbonatite Complex, SE Brazil: Fingerprinting fractional crystallisation and liquid immiscibility. In *Proceedings of the 8th International Kimberlite Conference: Extended Abstracts*, Victoria, BC, Canada, 22–27 June 2003; Volume 8.
47. Sun, S.; McDonough, W.F. Chemical and isotopic systematics of oceanic basalts: Implications for mantle composition and processes. In *Magmatism in the Ocean Basins*; Saunders, A.D., Norry, M.J., Eds.; Geological Society: London, UK, 1989; Volume 42, pp. 313–345.
48. Chakhmouradian, A.R.; McCammon, C.A. Schorlomite: A discussion of the crystal chemistry, formula, and inter-species boundaries. *Phys. Chem. Miner.* **2005**, *32*, 277–289. [[CrossRef](#)]
49. Ito, J.; Frondel, C. Synthetic zirconium and titanium garnets. *Am. Mineral.* **1967**, *52*, 773–781.
50. Zedlitz, O. Lime-iron garnets rich in titanium. *Zentralbl. Mineral. Geol. A* **1933**, 225–239.
51. Manning, P.G.; Harris, D.C. Optical absorption and electron-microprobe studies of some high-Ti andradites. *Can. Mineral.* **1970**, *10*, 260–271.
52. Laverne, C. Unusual occurrence of aegirine-augite, fassaite and melanite in oceanic basalts (DSDP Hole 504B). *Lithos* **1987**, *20*, 135–151. [[CrossRef](#)]
53. Melluso, L.; Srivastava, R.K.; Guarino, V.; Zanetti, A.; Sinha, A.K. Mineral compositions and petrogenetic evolution of the ultramafic-alkaline-carbonatitic complex of Sung Valley, northeastern India. *Can. Mineral.* **2010**, *48*, 205–229. [[CrossRef](#)]
54. Viladkar, S.G.; Wimmenauer, W. Geochemical and petrological studies on the Amba Dongar carbonatites (Gujarat, India). *Chem. Erde.* **1992**, *52*, 277–291.
55. Viladkar, S.G.; Bismayer, U. Compositional variation in pyrochlores of Amba Dongar carbonatite complex, Gujarat. *J. Geol. Soc. India* **2010**, *75*, 495–502. [[CrossRef](#)]
56. Magna, T.; Viladkar, S.; Rapprich, V.; Pour, O.; Hopp, J.; Čejková, B. Nb–V-enriched sövites of the northeastern and eastern part of the Amba Dongar carbonatite ring dike, India—A reflection of post-emplacement hydrothermal overprint? *Chem. Erde.* **2020**, *80*, 125534. [[CrossRef](#)]
57. Weber, H.P.; Virgo, D.; Huggins, F.E. A neutron diffraction and ^{57}Fe Mössbauer study of a synthetic Ti-rich garnet. In *Cambridge Institute Year Book*; Cambridge University: Washington, DC, USA, 1975; Volume 74, pp. 575–579.
58. Nicolescu, S.; Cornell, D.H.; Sodervall, U.; Odelius, H. Secondary ion mass spectrometry analysis of rare earth elements in grandite garnet and other skarn related silicates. *Eur. J. Mineral.* **1998**, *10*, 251–259. [[CrossRef](#)]
59. Whitney, P.R.; Olmsted, J.F. Rare earth element metasomatism in hydrothermal systems: The Willsboro-Lewis wollastonite ores, New York, USA. *Geochim. Cosmochim. Acta* **1998**, *62*, 2965–2977. [[CrossRef](#)]
60. Zhang, Y.; Liu, Q.; Shao, Y.; Li, H. Fingerprinting the hydrothermal fluid characteristics from LA-ICP-MS trace element geochemistry of garnet in the Yongping Cu deposit, SE China. *Minerals* **2017**, *7*, 199. [[CrossRef](#)]
61. Zhang, Y.; Shao, Y.J.; Wu, C.D.; Chen, H.Y. LA-ICP-MS trace element geochemistry of garnets: Constraints on hydrothermal fluid evolution and genesis of the Xinqiao Cu–S–Fe–Au deposit, eastern China. *Ore Geol. Rev.* **2017**, *86*, 426–439. [[CrossRef](#)]
62. Graunch, R.I. Rare earth elements in metamorphic rocks. In *Geochemistry and Mineralogical Rare Earth Elements*; Lipin, B.R., McKay, G.A., Eds.; De Gruyter: Berlin, Germany, 1989; Volume 21, pp. 146–167.

63. Mckay, G.A. Partition of rare earth elements between major silicate minerals and basaltic melts. In *Geochemistry and Mineralogy of Rare Earth Elements*; De Gruyter: Berlin, Germany, 1989; Volume 21, pp. 45–78.
64. Harris, N.B.W.; Gravestock, P.; Inger, S. Ion-microprobe determinations of trace-element concentrations in garnets from anatectic assemblages. *Chem. Geol.* **1992**, *100*, 41–49. [[CrossRef](#)]
65. Schwandt, C.S.; Papike, J.J.; Shearer, C.K.; Brearley, A.J. A SIMS investigation of REE chemistry of garnet in garnetite associated with the Broken Hill Pb–Zn–Ag orebodies, Australia. *Can. Mineral.* **1993**, *31*, 371–379. [[CrossRef](#)]
66. Bea, F.; Montero, P.; Garuti, G.; Zacharini, F. Pressure-dependence of rare earth element distribution in amphibolite and granulite-grade garnets. A LA-ICP-MS study. *Geostandard Newslett.* **1997**, *21*, 253–270. [[CrossRef](#)]
67. Bea, F.; Pereira, M.D.; Stroh, A. Mineral/leucosome trace-element partitioning in a peraluminous migmatite (a laser ablation-ICP-MS study). *Chem. Geol.* **1994**, *117*, 291–312. [[CrossRef](#)]
68. Hoal, K.E.O.; Hoal, B.G.; Erlank, A.J.; Shimizu, N. Metasomatism of the mantle lithosphere recorded by rare earth elements in garnets. *Earth Planet. Sci. Lett.* **1994**, *126*, 303–313. [[CrossRef](#)]
69. Skublov, S.G.; Drugova, G.M. REE Distribution in Metamorphic Garnets. Herald DGGGMS RAS 2. pp. 60–61. Available online: <http://geo.web.ru/conf/khitariada/5-2000.2/magm27.eng.pdf> (accessed on 12 July 2021).
70. Zhang, H.; Menzies, M.A.; Lu, F.; Zhou, X. Major and trace element studies on garnets from Paleozoic kimberliteborne mantle xenoliths and megacrysts from the North China craton. *Sci. China* **2000**, *D43*, 423–430. [[CrossRef](#)]
71. Boyd, F.R.; Pearson, D.G.; Hoal, K.O.; Hoal, B.G.; Nixon, P.H.; Kingston, M.J.; Mertzman, S.A. Garnet lherzolites from Louwrensia, Namibia: Bulk composition and P/T relations. *Lithos* **2004**, *77*, 573–592. [[CrossRef](#)]
72. Doroshkevich, G.A.; Viladkar, S.G.; Ripp, G.S.; Burtsera, V. Hydrothermal REE Mineralisation in the Amba Dongar Carbonatite Complex, Gujarat, India. *Can. Mineral.* **2009**, *47*, 1105–1116. [[CrossRef](#)]
73. Saha, A.; Ray, J.; Ganguly, S.; Chatterjee, N. Occurrence of melanite garnet in syenite and ijolite–melteigite rocks of Samchampi–Samteran alkaline complex, Mikir Hills, Northeastern India. *Curr. Sci.* **2011**, *101*, 95–100.
74. Masuda, A.; Lkeuchi, Y. Lanthanide tetrad effect observed in marine environment. *Geochem. J.* **1979**, *13*, 19–22. [[CrossRef](#)]
75. Peretyazhko, I.S.; Savina, E.A. Tetrad effects in the rare earth element patterns of granitoid rocks as an indicator of fluoride–silicate liquid immiscibility in magmatic systems. *Petrology* **2010**, *18*, 514–543. [[CrossRef](#)]
76. Doelter, C. Granatgruppe. In *Handbuck der Mineralchemie: Bd.II (1915–1917)*; Springer: Berlin/Heidelberg, Germany, 1916; pp. 878–915.
77. Badalov, S.T. Vanadium-bearing tourmaline and garnet Zafiski Vsesoyuz. *Minerol. Obs.* **1951**, *80*, 212–213.
78. Mariano, A.N. Nature of economic mineralization in carbonatites and related rocks. In *Carbonatites: Genesis and Evolution*; Unwin Hyman: London, UK, 1989; pp. 149–176.
79. Bau, M. Rare-earth element mobility during hydrothermal and metamorphic fluid–rock interaction and the significance of the oxidation state of europium. *Chem. Geol.* **1991**, *93*, 219–230. [[CrossRef](#)]
80. Migdisov, A.; Williams-Jones, A.E.; Brugger, J.; Caporuscio, F.A. Hydrothermal transport, deposition, and fractionation of the REE: Experimental data and thermodynamic calculations. *Chem. Geol.* **2016**, *439*, 13–42. [[CrossRef](#)]
81. Migdisov, A.A.; Williams-Jones, A.E. Hydrothermal transport and deposition of the rare earth elements by fluorine-bearing aqueous liquids. *Miner. Depos.* **2014**, *49*, 987–997. [[CrossRef](#)]
82. Williams-Jones, A.E.; Migdisov, A.A.; Samson, I.M. Hydrothermal mobilisation of the rare earth elements—A tale of “ceria” and “yttria”. *Elements* **2012**, *8*, 355–360. [[CrossRef](#)]
83. Allen, D.E.; Seyfried, W.E. REE controls in ultramafic hosted MOR hydrothermal systems: An experimental study at elevated temperature and pressure. *Geochim. Cosmochim. Acta* **2005**, *69*, 675–683. [[CrossRef](#)]
84. Roedder, E. Fluid inclusions from the fluorite deposits associated with the carbonatite of Amba Dongar, India and Okorusu, south west Africa. *Trans. Inst. Min. Metal.* **1973**, *82*, B35–B39.
85. Simonetti, A.; Bell, K. Nd, Pb, and Sr isotope systematics of fluorite at the Amba Dongar carbonatite complex, India: Evidence for hydrothermal and crustal fluid mixing. *Econ. Geol.* **1995**, *90*, 2018–2027. [[CrossRef](#)]
86. Srivastava, R.K.; Taylor, L.A. Carbon-and oxygen-isotope variations in Indian carbonatites. *Int. Geol. Rev.* **1996**, *38*, 419–429. [[CrossRef](#)]
87. Viladkar, S.G.; Schidlowski, M. Carbon and oxygen isotope geochemistry of the Amba Dongar carbonatite complex, Gujarat, India. *Gondwana Res.* **2000**, *3*, 415–424. [[CrossRef](#)]
88. Ray, J.S.; Ramesh, R. Stable carbon and oxygen isotopic compositions of Indian carbonatites. *Intl. Geol. Rev.* **2006**, *48*, 17–45. [[CrossRef](#)]
89. Hopp, J.; Viladkar, S.G. Noble gas composition of Indian carbonatites (Amba Dongar, Siriwasan): Implications on mantle source compositions and late-stage hydrothermal processes. *Earth Planet. Sci. Lett.* **2018**, *492*, 186–196. [[CrossRef](#)]